ELSEVIER

Contents lists available at ScienceDirect

Combustion and Flame

journal homepage: www.elsevier.com/locate/combustflame



Small aromatic hydrocarbons control the onset of soot nucleation



Kevin Gleason^a, Francesco Carbone^{a,b}, Andrew J. Sumner^c, Brian D. Drollette^c, Desiree L. Plata^{c,d}, Alessandro Gomez^{a,*}

- ^a Department of Mechanical Engineering and Materials Science, Yale University, 9 Hillhouse Avenue, New Haven, CT 06520, United States
- ^b Department of Mechanical Engineering, University of Connecticut, 191 Auditorium Road, Unit 3139, Storrs, CT 06269, United States
- Department of Chemical and Environmental Engineering, Yale University, 17 Hillhouse Avenue, New Haven, CT 06520, United States
- ^d Department of Civil and Environmental Engineering, Massachusetts Institute of Technology, 77 Massachusetts Avenue, Cambridge MA 02139, United States

ARTICLE INFO

Article history:
Received 15 May 2020
Revised 17 August 2020
Accepted 17 August 2020
Available online 27 October 2020

Keywords:
Polycyclic aromatic hydrocarbons
Soot
Flames
Capillary-sampling
Gas chromatography

ABSTRACT

The gas-to-particle transition is a critical and hitherto poorly understood aspect in carbonaceous soot particle formation. Polycyclic Aromatic Hydrocarbons (PAHs) are key precursors of the solid phase, but their role has not been assessed quantitatively probably because, even if analytical techniques to quantify them are well developed, the challenge to adapt them to flame environments are longstanding. Here, we present simultaneous measurements of forty-eight gaseous species through gas capillary-sampling followed by chemical analysis and of particle properties by optical techniques. Taken together, they enabled us to follow quantitatively the transition from parent fuel molecule to PAHs and, eventually, soot. Importantly, the approach resolved spatially the structure of flames even in the presence of steep gradients and, in turn, allowed us to follow the molecular growth process in unprecedented detail. Noteworthy is the adaptation to a flame environment of a novel technique based on trapping semi-volatile compounds in a filter, followed by off-line extraction and preconcentration for quantitative chemical analyses of species at mole fractions as low as parts per billion. The technique allowed for the quantitation of PAHs containing up to 6 aromatic rings. The principal finding is that only one- and two-ring aromatic compounds can account for soot nucleation, and thus provide the rate-limiting step in the reactions leading to soot. This finding impacts the fundamental understanding of soot formation and eases the modeling of soot nucleation by narrowing the precursors that must be predicted accurately.

 $\ensuremath{\mathbb{C}}$ 2020 The Combustion Institute. Published by Elsevier Inc. All rights reserved.

1. Introduction

The emission of carbonaceous particles (i.e., soot) is a problem that has been plaguing humans for centuries, with repercussions on health [1–3] and climate [4,5] that have been appreciated only in recent decades. It is dominant in fires that are linked to global warming [6] and it affects combustion technologies that are responsible for more than 80% of the total energy conversion worldwide, with their dominance unlikely to subside in the foreseeable future [7]. As a result, soot is the second most significant contributor to radiative forcing in climate change [4,5]. Even if stringent regulations have curtailed the emissions of large soot particles, the health impact remains unabated because of the reported increased toxicity of nanosized materials [8–10], sorbed toxic semi-volatile compounds, and their ability to reach deep in the respiratory tract [1]. In addition to its broad importance from a terrestrial perspective, the formation at high temperature of the carbonaceous or-

ganic molecules and interstellar dust is a topic of astrophysical relevance that is yet to be clarified [11,12].

Soot formation in flames occurs through a series of chemical and physical transformations, which include decomposition of the fuel and subsequent pyrolytic growth forming progressively larger Polycyclic Aromatic Hydrocarbons (PAHs) that are eventually converted into particle nuclei [13–26]. The critical missing link to a fundamental understanding of soot formation is precisely this gas-to-particle transition (i.e., nucleation) [22–27]. Nucleation contributes modestly *per se* to soot mass, but the nuclei are ultimately the site on which surface growth occurs, and surface growth is responsible for the bulk of the soot formed in flames [13,16,17,19,21,26].

A crucial step in the growth process starting with non-cyclic aliphatic fuels is the formation of the first aromatic ring, a benzene molecule [17–21,26]. Growth to larger aromatic molecules includes a set of sequential reactions, such as those considered in the Hydrogen Abstraction Carbon Addition (HACA) mechanism [14,17,19,21,26] and those involving resonantly stabilized radicals [18,20,24,27]. The involvement of conjugated compounds with al-

^{*} Corresponding author.

E-mail address: Alessandro.Gomez@Yale.edu (A. Gomez).

ternating single and multiple bonds is needed for the soot precursor to have the stability to withstand the flame high temperatures [16,28]. The formation mechanisms of small PAHs composed of one and two rings are relatively well understood, and the estimates of the relevant kinetic parameters are supported by experimental data [29-33]. In contrast, understanding the growth to larger ring structures has been stymied by analytical challenges. Efforts to quantify larger PAHs are rare and data typically do not include species larger than pyrene (202 amu), because of the low abundance of these larger structures in flames. For example, an order-of-magnitude reduction in abundance is anticipated for every additional ring [15,23,28], rapidly eliminating structures with more than a few rings out of the viable analytical window of most mass spectral detectors. While some PAHs have been detected using molecular-beam photoionization mass spectrometry [29,30], these measurements rely on highly intrusive sampling probes [34-37] that cannot resolve the structure of flames with sharp gradients. Additionally, the quantitation of species relies on estimates of the sampling flow rate and of the ionization efficiencies [29].

Since reaction kinetics forming large PAHs are not quantitatively established, the soot inception step is often modeled heuristically by considering the dimerization of PAHs with reaction rates that are tuned to match experimentally measured soot volume fraction and particle size [17]. Such a tuning is empirical and applies, at best, under restricted flame conditions. Quantitative, spatiallyresolved, and minimally intrusive measurements of both gaseous species and soot volume fraction in either a counterflow diffusion/partially premixed flame (e.g., [29-33]) or a premixed flame [38] are available, but are limited to species composed of two-ring aromatics or smaller. Here, we provide the first spatially-resolved measurements of (i) PAHs composed of up to 6 rings, including some of the reputed critical soot precursors, in addition to (ii) soot particle size and number concentration, using a combination of soot pyrometry and light scattering. Specifically, we track the evolution from parent molecule to multi-ring PAHs and, ultimately, soot in a highly controlled flame under incipient soot conditions, to ensure compatibility of the diagnostics with soot load. As a result, we obtain unprecedented knowledge of the soot nucleation stage in an environment that is convenient to track the history of evolution from fuel to soot along a streamline. To accomplish this goal, we leveraged a capillary-sampling approach that retains the necessary spatial resolution to resolve the structure of a variety of flame environments, even at high pressures [39,40], and combined it with a trapping and preconcentration technique, to analyze quantitatively a series of PAHs at mole fractions as low as one part per billion [41,42]. By having a direct comparison of the spatial sequencing of the number concentration of aromatic compounds and soot particles, as well as their respective production rates, one can assess which PAHs control the soot nucleation rate. Ultimately, this approach enables the determination of the minimum assessment criteria and model requirements to describe soot nucleation accurately and could have far-reaching impacts on our ability to describe one of Earth's oldest and most dominant material transformation processes.

2. Experimental procedure

2.1. Burner

Experiments are performed in an atmospheric pressure counterflow diffusion flame [31–33]. The bottom jet is composed of an ethylene/nitrogen mixture (0.330/0.670 by mole fraction) with nominal mass averaged velocity of 20.2 cm/s (at 298 K), whereas the top counterflowing stream contains an oxygen/nitrogen mixture (0.229/0.771 by mole fraction) with a nominal velocity of 19.8 cm/s (at 298 K). The jets are generated in two identical con-

verging nozzles with an internal outlet diameter of 6.35 mm [39,40], which are oriented in an opposed flow configuration and separated by 8 mm. Each nozzle is equipped with a conical enclosure to flow nitrogen, shielding the flame from external disturbances. The investigated flame is steady, laminar, and one-dimensional along the burner axis where measurements are performed.

2.2. Capillary sampling

Gaseous samples are collected using capillary tube probes inserted radially into the flame with the tip positioned slightly off-axis at various axial distances from the burner nozzles. Capillary tubes of different materials and outer/inner diameters are used to verify the independence of the results from sampling intrusiveness artifacts. In particular, the capillary probe is made of either a silica (outer/inner diameter of either 360/150 μm or 150/100 μm) or a 316 stainless steel (340/180 μm) tube. The outlet of the capillary probe is kept under vacuum at a pressure below 350 Torr to extract samples under choked flow conditions.

Sampling procedures are unavoidably perturbative and introduce biases, including flame perturbations, because of the probe intrusiveness and chemical modification of the sampled gas. However, the use of capillary probes to sample gaseous species from flames has been shown to be robust under a wide range of flame conditions [31,33,39,40]. Inserting the probe inevitably causes a fluid dynamic perturbation that "drags" the flame. The effect can be corrected by measuring optically the distance between the probe tip and the flame blue chemiluminescence, whose position corresponds to the maximum concentration of CH*. This approach allows us to overlap the experimental data with the model predictions and enables spatially-resolving flames with even sharper concentration gradients than those in the present flame [39,40]. As reviewed in [43], sampling probes often rely on aerodynamic quenching to minimize chemical reactions occurring within the probe at the cost of losing spatial resolution and severely distorting the temperature and flow field [29,34-37]. The use of extremely thin capillary probes minimizes the thermal perturbation of the flame and the remaining issue is associated only with the steadystate energy balance of the radiative losses at the surface of the probe. The capillary probe extracts samples from the flame under sonic conditions. The substantial quenching of the reactions occurring within the probe was assessed with chemical kinetic modeling by considering the most severe temperature and pressure conditions within the sampling probe. It resulted in a change of the mole fraction smaller than the experimental uncertainty

2.3. Chemical analysis - Method 1: direct capillary sampling

To quantify species up to three-ring aromatics, we follow a well-established method that demonstrated robustness under a wide range of flame conditions [31,38,39]. Extracted gaseous samples are temporarily stored in a sampling loop, heated to 423 K to avoid condensation of heavier species, and subsequently injected into a Gas Chromatograph (GC, Agilent 6890A) equipped with three detectors used to quantify the species of interest. A thermal conductivity detector (TCD) measures H2, N2, O2, and CH4; a flame ionization detector (FID) following a methanizer measures CO, CO₂, CH_4 , C_2H_2 , C_2H_4 , and C_2H_6 ; and a mass spectrometer (MS, Agilent 5973 N) quantifies hydrocarbons composed of three or more carbon atoms including polycyclic aromatic hydrocarbons (PAH) composed of up to three aromatic rings. The limit in detecting even larger species with this technique is dictated by condensation losses in the sampling system and the vanishingly small concentrations that bring the signal below the detection limit of the MS. Calibrations of the measured signals are performed with various Scotty Specialty Gas calibration mixtures. Heavier species (C_5 and larger) are calibrated using liquid mixtures containing all compounds of interest. The liquid mixture is atomized with an electrospray into a heated stream of nitrogen, producing a gaseous stream of known concentration. The calibration error is estimated to be within 5% using calibration bottles and $\pm 15\%$ for heavier species (larger than C_5).

2.4. Chemical analysis - Method 2: preconcentration techniques

To quantify PAHs composed of up to 6-rings whose concentrations are too low to be accurately measured with traditional methods, we follow "Method 2" relying on an enrichment procedure that has been established in a different context [41,42,44]. A low volume polyurethane foam (PUF) filter, 22 mm in diameter and 76 mm in length, is inserted in the sampling line, immediately downstream of the capillary probe. The PUF captures PAHs from the flame sampled gas over an extended time interval (on the order of 1 h per sampling location). During sampling, the PUF is kept at room temperature and approximately 300 Torr to ensure that the sampling probe continues to operate under choked flow conditions. Choked flow is critical to maintain a constant molar flow rate through the PUF and readily convert the collected mass of PAHs to a concentration based on the sampling time. The molar flow rate is measured directly by connecting the sampling line to a large volume vessel evacuated before the measurements and whose pressure rate of change is recorded during the sampling time. A linear increase in pressure confirms that a constant molar flow rate (i.e., choked flow) is achieved when keeping the pressures downstream of the PUF at 300 Torr. After the sampling, the PUF and (externally precleaned) PUF holder, capillary probe, and intermediate connection fittings are submerged in a 100-mL cell of dichloromethane at 1000 psi and 100 °C for 7 min using a Dionex accelerated solvent extractor (ASE) and subsequently rinsed with clean dichloromethane. The procedure allows the extraction of the material captured during the flame sampling and disperses/solubilizes it in dichloromethane. It is repeated three times to maximize the extraction efficiency. The same triplicate procedure is used before the flame sampling to clean all the components. Analysis of the materials extracted from clean sampling components is used to rule out contaminations of the results due to the experimental extraction procedure. The extracted dichloromethane solution is spiked with a known amount of deuterated internal standards $(d_4$ –1,4-dichlorobenzene, d_8 -naphthalene, d_{10} -acenaphthene, d_{10} phenanthrene, d_{12} -chrysene, and d_{12} -perylene) and concentrated to approximately 1 mL by rotary evaporation before being injected in the GCxGC/MS system (Leco Pegasus 4D GCxGC-TOF-MS) used for the analysis. The spiking of the sample with deuterated standards is used for calibration purposes. Sample extraction efficiency is assessed using a recovery standard (p-terphenyl- d_{14}) and found to be over 85%. Volatile compounds (hydrocarbons smaller than tworing aromatics) have poor collection efficiencies onto the PUF and are lost during rotary evaporation; thus, those were not quantified with this method. Method 2 can be used reliably only to quantify species with boiling temperatures larger than ~410 K, including all aromatic species composed of at least two rings and has a detection limit of concentration of approximately 1 ppb. Here, we note that the high collection and extraction efficiency pertains to compounds containing more than two aromatic rings, including all isomers, or polyaromatic species that are alkylated or contain heteroatoms [41,45,46]. Similarly, the mass spectrometric method does not preclude the detection of any isomers or substituted aromatic hydrocarbons: they are all detectable if present above approximately 1 ppbv. We note that such a 'limit' is due to the length of sampling time: in principle it can quantify species at concentrations below 1 ppb by collecting samples over an even longer time interval, so long as flame stability and probe clogging are not problematic

2.5. Pyrometry

Non-intrusive soot pyrometry measurements are performed by imaging the flame onto a Nikon D70 camera with a 210 mm focal length lens stopped at f/8. Measurements are performed by averaging 20 images after overlapping the blue chemiluminescence of each image. Images are split into the red, green, and blue color channels and deconvolved into a two-dimensional field using an Abel transform. According to Plank's law, the ratio of any two deconvolved color channels, S, can be expressed as

$$\frac{S_i}{S_j} = \frac{\int \eta_i(\lambda) \ \lambda^{-(\alpha+5)} \left[\exp\left(\frac{hc}{\lambda k_B T}\right) - 1 \right]^{-1} d\lambda}{\int \eta_j(\lambda) \ \lambda^{-(\alpha+5)} \left[\exp\left(\frac{hc}{\lambda k_B T}\right) - 1 \right]^{-1} d\lambda},\tag{1}$$

where λ , h, c, k_B , and α are the wavelength, Plank constant, speed of light, Boltzmann constant, and dispersion exponent, respectively. The subscripts *i* and *j* represent anyone of the three color channels. The CCD sensor spectral response and transmission losses through both the camera lens and pressure-chamber window are accounted for in $\eta(\lambda)$; the spectral response of the sensor is approximately between 375 nm and 700 nm [47]. The dispersion exponent, α , is related to the soot carbon-to-hydrogen (C/H) ratio [48,49] and arises from the power-law dependence of the extinction coefficient. Assuming that scattering is negligible compared to absorption and that soot absorptivity is equal to emissivity (i.e., Kirchhoff's law) ultimately leads to the soot emissivity $\in \propto K_{ext} \propto \lambda^{-\alpha}$ [32,38,48]. Soot particles are assumed to be in thermal equilibrium with the gas phase and the temperature of the gas phase is based on onedimensional modeling that has been validated by gaseous species measurements and thermocouple measurements [31-33]. Consequently, the measured ratio of any two color channels is used to evaluate the dispersion exponent in Eq. (1). Soot volume fraction is evaluated through

$$f_{\nu} = -\frac{\lambda_{e}}{\tilde{K}_{ext}L_{p}} \ln \left\{ 1 - \epsilon_{c}(\lambda_{e}) \frac{\tau_{c}S_{s}}{\tau_{s}S_{c}} \exp \left[-\frac{hc}{k_{B}\lambda_{e}} \left(\frac{1}{T_{c}} - \frac{1}{T_{s}} \right) \right] \right\}, \quad (2)$$

where λ_e , \tilde{K}_{ext} , L_P , and τ are the effective wavelength of the color channel, dimensionless extinction coefficient, pixel length, and exposure time, respectively. We assume a constant $\tilde{K}_{ext} = 5.34 \pm 2.68$ [32]. The subscripts c and s refer to the calibration and measurements on soot particles, respectively. A S-type thermocouple is used as a light calibration source [50].

2.6. Light scattering

For the light scattering measurements, the second harmonic of a 10-ns pulse Nd-Yag laser at 532 nm is shaped into a 4 mm \times 1 mm beam and imaged with an optical train, including lenses, a polarizer, and a 10-nm bandwidth interference filter, onto an intensified camera (PCO DiCAM-Pro) positioned at a 90 deg scattering angle. The camera uses a 20 ns gating time. Measurements are repeated at multiple laser fluences in the 20–70mJ/cm² range. Rayleigh scattering calibrations are performed with nitrogen, ethylene, and propane to verify that the expected scattering ratio is achieved. The gas-phase Rayleigh scattering coefficient is calculated using the computed temperature and mole fraction of the most abundant species with known scattering cross-sections (i.e., H₂, H₂O, N₂, O₂, CH₄, CO, CO₂, C₂H₂, C₂H₄, C₂H₆, C₃H₈, C₃H₄, C₄H₆, and C_6H_6 [51–53]) which account for more than 99% of the flame molar composition at any position in the flame. Measurements and calculations overlap in the regions devoid of soot, whereas an excess light scattering is detected in the soot laden region of the flame.

The number concentration of soot, N_S , is calculated as

$$N_{\rm S} = \frac{9\pi^2 F(m) f_{\nu}^2}{Q_{\nu\nu}^{\rm soot} \lambda^4},\tag{3}$$

where Q_{vv}^{soot} is the measured excess scattering coefficient attributed to soot, net of the Rayleigh scattering contribution from the gas phase [51], f_v is the measured soot volume fraction via pyrometry, and F(m)=0.69±0.13 is the dimensionless refractive index function at the laser wavelength λ = 532 nm [54]. The error bars on the measured soot number concentration is based on error propagation by applying general uncertainty analysis to Eq. (3).

3. Modeling and data analysis

3.1. Computational

The structure of the flame is computed using one-dimensional governing equations. The used chemical kinetic and transport model is described in [55]. It was found to perform reasonably well even for relatively large aromatics that other models do not include. Computations are performed using the CHEMKIN interpreter [56] coupled to the OPPDIF code [57]. A multicomponent determination of the diffusion coefficients and thermal diffusion are included in all computations. Heat losses by radiation of CH₄, CO, CO₂, and H₂O in the optically thin limit are considered when solving the energy equation [58]. We rely on a combination of experimental thermocouple measurements and simulations using a two-dimensional COMSOL model [31,33] to impose correct boundary conditions accounting for deviations from the ideal plug flow at the exit of the nozzles. The use of these modified boundary conditions does not affect the computed temperature profile, as independently validated with thermocouple measurements [31-33], but has a non-negligible impact on the computed profiles of polycyclic aromatic hydrocarbons (PAHs) with slow formation kinetics [40].

3.2. Production rates

The soot production rate is recovered from the governing equation for the number concentration N_s of soot particles along the axis, z, of the axis-symmetric flow field, namely,

$$\frac{\partial N_{S}}{\partial t} \Big|_{nucl} - \left. \frac{\partial N_{S}}{\partial t} \right|_{coag}$$

$$= \frac{d}{dz} (N_{S} \cdot V_{z}) + N_{S} \cdot \frac{d V_{r}}{dr} + \frac{d}{dz} (N_{S} \cdot V_{th}) + \frac{d}{dz} (N_{S} \cdot V_{P}) \tag{4}$$

The first term on the LHS of Eq. (4) is the number concentration production rate from the gas phase (i.e., nucleation rate) and the second term is the destruction rate due to coagulation of particles, $\frac{\partial N_S}{\partial t}|_{coag} = \gamma_{coag} \frac{1}{2} K_{coll} N_S^2$, with K_{coll} as collision kernel and γ_{coag} as coagulation efficiency (probability that once particles collide, they stick together) [22,59,60]. The four terms on the RHS are the two convective terms, the thermophoretic contribution due to particle drift down a temperature gradient and the diffusive term due to the particle Brownian motion, respectively [61-63]. V_z , V_r , V_{th} and V_P are the axial velocity component, the radial velocity component, the thermophoretic velocity, and the particle Brownian velocity, respectively. In this equation N_s is experimentally determined under the assumption of particle monodispersity, whereas the velocity terms are extracted reliably from the computational model, along with kinematic gas viscosity, ν , density, ρ , and temperature, T, given the excellent agreement between experiments and computed variables (see Fig. 1(B)).

In Eq. (4), diffusive terms include the thermophoretic velocity, $V_{th} = -0.538 \cdot v \frac{d}{dz} ln(T)$ and the particle Brownian velocity, $V_P = -0.538 \cdot v \frac{d}{dz} ln(T)$

 $-D_P \frac{d}{dz} ln(N_S)$. The average value of the Brownian diffusivity, D_P used in Eq. (4), is calculated as a function of the measured average particle diameter, d, and of an assumed density for soot ρ_S =1.5 g/cm³:

$$D_{P} = \left(\frac{k_{B}T}{3\pi \rho_{s} \nu d}\right) \left[1 + 2Kn\left(A + B e^{-\frac{c}{Kn}}\right)\right],\tag{5}$$

In Eq. (5) the Knudsen number, *Kn*, is the ratio of gas mean free path to particle diameter, A, B, and C are empirical constants set equal to 1.257, 0.4, and 0.55, respectively [61].

The collision kernel, K_{coll} , in Eq. (4) is calculated by assuming either monodispersity or lognormal distribution of the soot particle sizes to integrate over the size distribution. With a formula that is valid in both free-molecular (Kn >> 1), transition ($Kn \sim 1$) and continuum regimes (Kn << 1) [61]:

$$K_{coll} = 8\pi d \cdot D_{P} \left\{ \frac{d}{d + \sqrt{2} \cdot g} + \frac{8 D_{P}}{\sqrt{2}c \cdot d} \right\},$$
with $g = \frac{\pi c}{24d \cdot D_{P}} \left\{ \left(d + \frac{8D_{P}}{\pi c} \right)^{3} - \left[d^{2} + \left(\frac{8D_{P}}{\pi c} \right)^{2} \right]^{3/2} \right\} - d,$
and $c = \sqrt{\frac{48k_{B}T}{\pi^{2} \rho_{c} d^{3}}}.$ (6)

To estimate the dimerization rate of aromatics, we use the selfcollision rate from kinetic theory according to

$$\dot{\omega}_{\text{DIM}} = \eta \sqrt{\frac{4\pi k_B T}{M_{PAH}}} \sigma^2 \Omega^*(T^*) N_a^2 [PAH]^2, \tag{7}$$

where η , k_B , N_a , M_{PAH} , σ , $\Omega^*(T^*)$ are the dimerization efficiency, Boltzmann constant, the Avogadro number, the mass, the collision diameter, and the reduced collision integral [64] of the PAH in question. $\dot{\omega}_{DIM}$ represents the number of dimers generated per unit volume and time from the self-collisions of the considered PAH at concentration [PAH]. The self-collision production rate is estimated by interpolating the experimental measurements of [PAH] and assumes a high probability of dimerization with $\eta=0.01$. Of course, Eq. (7) can be generalized beyond self-collision to the collision of any two aromatics.

4. Results and discussion

Figure 1(A) shows a true-color photograph of the counterflow diffusion flame with marked Gas Stagnation Plane (GSP) at the interface of the two streams, which defines the zero position of the axial coordinate, z. The fuel and oxygen sources enter from left and right, respectively. The flame is stabilized on the oxidizer side of the GSP, as indicated by the blue chemiluminescence of its front. The faint one-mm thick orange-yellow luminosity is due to soot natural incandescence. Note that the image has been rotated 90° counterclockwise to maintain a consistent orientation with the adjacent panels, and the image strip above each panel shows the sampled region of the flame near its axis. The flame is flat and its structure in proximity of the burner axis depends only on the distance from the GSP, with inconsequential two-dimensional effects confined to the flame edges (i.e., the top and bottom of the photograph).

Figure 1(B) shows spatial profiles of temperature and major species, where the symbols represent measurements and the lines represent modeled results. Diffusion flames are characterized by sharp spatial gradients in the mixing zone between the fuel and oxidizer. The sampling technique deployed here is able to resolve these gradients and provides the characterization of the flame at a resolution on the order of 100 µm or finer, depending on the choice of capillary probe diameter [40]. The selected counterflow flame

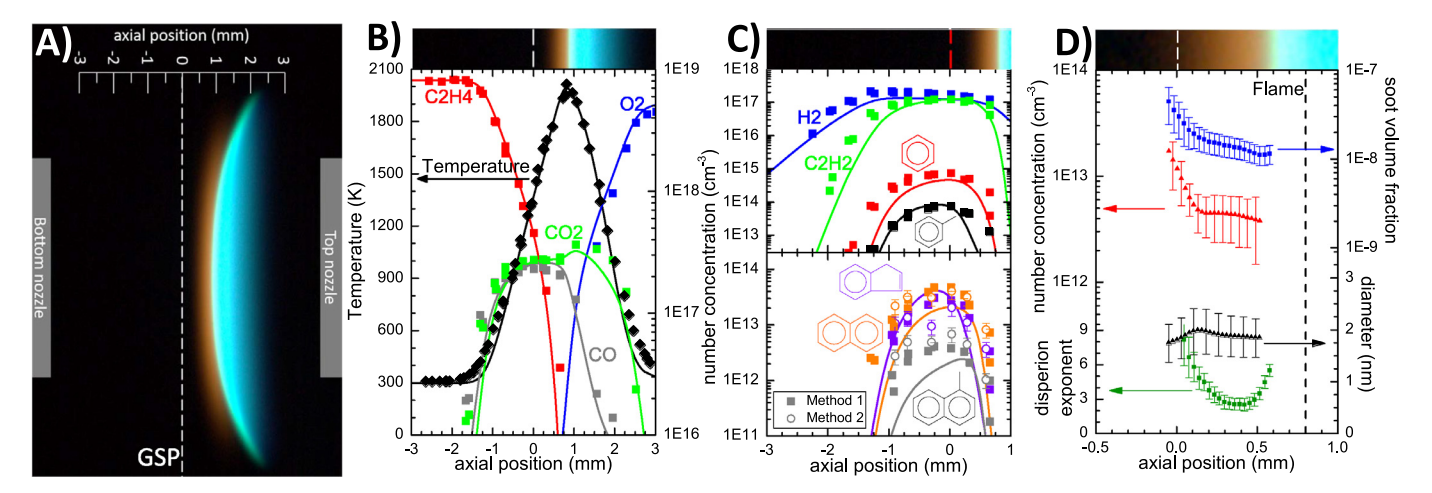


Fig. 1. (A) Photograph of the counterflow diffusion flame with marked gas stagnation plane at the interface of the two streams. (B) Spatial profiles of temperature and major species. (C) Profiles of selected species relevant to soot chemistry: H_2 , C_2H_2 , benzene and toluene (top panel); indene, naphthalene, and lumped 1-methyl-naphthalene (bottom panel), as obtained with conventional gas microsampling (Method 1, full symbols) and its filter trapping variance (Method 2, open symbols); (D) Soot characterization in terms of volume fraction, number concentration, particle size and dispersion exponent.

has a peak temperature of approximately 1980 K and sharp temperature and compositional gradients in the parent fuel (ethene; C_2H_4), oxygen (O_2) , carbon dioxide (CO_2) , and carbon monoxide (CO). Downstream of the flame front (i.e., away from the oxygen source and for positive values of the abscissa), purely pyrolytic conditions prevail, because of the rapid consumption of oxygen at the flame front, with the occurrence of PAH growth and soot formation. As expected, for low molecular weight species model predictions are in very good agreement with measurements.

Profiles of selected species relevant to soot chemistry are shown in Fig. 1(C): H_2 , C_2H_2 , benzene and toluene (top panel); indene, naphthalene, and lumped 1-methyl- and 2-methyl-naphthalene (bottom panel), as obtained with conventional gas capillary-sampling (Method 1, full symbols) and filter trapping (Method 2, open symbols). Error bars represent the standard deviation of triplicate injections. The smallest important soot building block generated by the flame, acetylene, forms early in the fuel region and progressively increases, as does hydrogen, while being convected toward the GSP before decreasing as it diffuses beyond the GSP towards the flame.

Other key soot precursors, one- and two-ring aromatic compounds, have more compressed spatial profiles and their experimental abundances are also in good agreement with computational predictions. Two-ringed aromatic compounds present a unique opportunity for intercomparison of the novel technique required for the larger PAHs (Method 2) with the better established method relying on flame sampling through a capillary probe and quantification of gaseous species by direct injection of the sample into the GC/MS (Method 1) (e.g., [31,33,38]). In Method 2 the preconcentration step is critical to obtain the sensitivity required for the trace concentrations of aromatic species present in flames and has been deployed in other systems previously [41,42,44]. Nevertheless, it requires validation using species that are detected with both methods to demonstrate consistency. Both methods gave measured concentrations of indene, naphthalene, and summed 1-methyl- and 2methyl-naphthalene that agreed within experimental uncertainty (Fig. 1(C), bottom). Since the preconcentration techniques can be used to interrogate species with boiling temperatures above 410 K, including two-ringed aromatics, at low detection limits (down to approximately 1 ppb), this independent confirmation builds confidence in the approach to bridge a longstanding experimental gap between few and multi-ring aromatic species on the path to incipient soot.

The soot particle field of the counterflow flame was characterized using established methods and is shown in Fig. 1D in terms

of volume fraction, number concentration, particle size and dispersion exponent from pyrometry and light scattering measurements. The number concentration is calculated by assuming size monodispersity, which results in a lower estimate. The volume fraction was determined using multi-color pyrometry coupled with fine thermocouple measurements [32,38], whereas particle size and number density were inferred by laser light scattering in combination with pyrometry. Size monodispersity results in the smallest values of the number density: if one assumes a log-normal distribution, keeping constant the experimentally measured soot volume fraction and scattering signal, the number concentration would *increase* with increasing standard deviation (σ) of the logarithm of particle diameter [65] by as much as a factor of three for σ =0.25, independently of the axial position.

The number concentration and particle diameter remain nearly constant as the particles are convected toward the GSP (i.e., away from the flame). Near the GSP, the number concentration and soot volume fraction increase measurably, suggesting an additional soot nucleation mechanism in this region of low oxygen, higher fuel availability, and coincident with peak concentrations of oneand two-ring aromatic compounds. This enhanced soot formation occurs where temperatures have drastically decreased to 1100-1300 K, just 500 µm from the flame front, again suggestive of a distinct and unique soot formation pathway. Note that the detection of soot extends beyond the GSP: soot particles "punch" through the gas stagnation plane, propelled by thermophoretic transport down the temperature gradient, and define a Particle Stagnation Plane (PSP) approximately 200 µm to the left of the GSP, beyond which no soot is present. A confirmation of these dynamics can be inferred from the soot dispersion exponent, α , which serves as a proxy for the age of soot particles (Fig. 1(D)) [38,48,49]. Younger or newly formed soot has low carbon-to-hydrogen (C/H) ratios and correspondingly large α , whereas older soot has undergone more dehydrogenation, corresponding to higher C/H ratios and lower α . The behavior of α indeed confirmed the existence of two distinct regions for particle inception: the "high-temperature" soot formation zone close to the flame and the "low-temperature" formation zone close to the PSP [32].

The question arises as to what drives these two unique formation zones and if the construction of sequentially larger aromatic structures *must* precede the formation of soot [19–24]. However, elusive detection of these larger ringed aromatic compounds has prevented a quantitative experimental evaluation of this hypothesis. Here, we present the number concentration of single-to-6-ringed aromatic structures (e.g., benzo[a]pyrene and

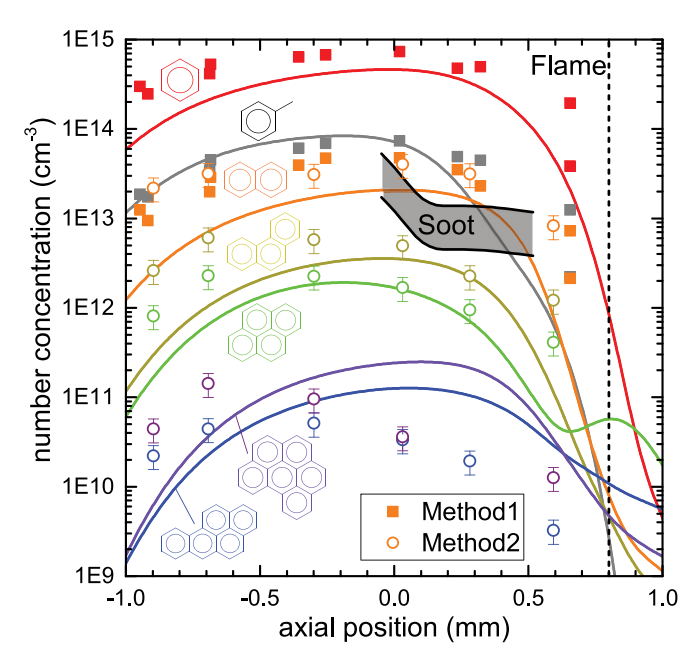


Fig. 2. Number concentration profiles of soot (gray shaded area) and selected aromatic compounds (colored symbols and lines for measurements and model, respectively) ranging from the single-ring benzene to 6-ring benzo[ghi]perylene. The soot shaded area includes the experimental uncertainty and is bound by values calculated assuming either particle monodispersity (lower black line) or a lognormal size distribution with a relative standard deviation equal to 0.25 (upper black line). Data for the two-ring aromatic are represented by filled symbols if collected by direct capillary measurement (Method 1), whereas open symbols refer to measurements via trapping and preconcentration techniques (Method 2). (For interpretation of the references to color in this figure legend, the reader is referred to the web version of this article.)

benzo[ghi]perylene) and compare them with the number concentration of soot (Fig. 2). Over 24 polyaromatic species, including methylated and ethylated structures, were explicitly measured, along with 24 additional monoaromatic compounds and other small precursors and by-product gases (see Supplemental Materials (SM)). In particular, five-membered PAHs were detected at comparable concentration levels as 6-membered PAHs of similar molecular weight, but are listed only in the SM since most of them are not included in chemical kinetic model [55] for comparison. Data for the two-ring aromatic are represented by filled symbols for direct capillary sampling measurements (Method 1), whereas open symbols show measurements via the trapping and preconcentration technique (Method 2). Resolving the sharp concentration gradients in the counterflow flame and quantifying species spanning more than 6 orders of magnitude in concentration attest to the capability of the experimental approach.

There is generally good agreement between the experimental results and chemical abundance predictions using the chemical model for small aromatic species (Figs. 1 and 2), but for larger aromatic compounds, differences in the modeled and experimental results can be as large as a half to a full order of magnitude, especially in the soot nucleation zone of the flame. This difference is exacerbated for structures beyond three- or four-rings, suggesting that updates to the kinetic descriptors for large aromatic structures are needed in order to predict accurately their formation in relevant combustion processes. The present data will inform such modeling by providing a benchmark for model validation. The necessity of the fine spatial resolution is evident in the measurements.

The fact that the applied diagnostics only measure *stable* molecules does not introduce significant bias. In fact, transient radical species are expected to exist at concentration one or two orders of magnitude smaller than their respective stable counter-

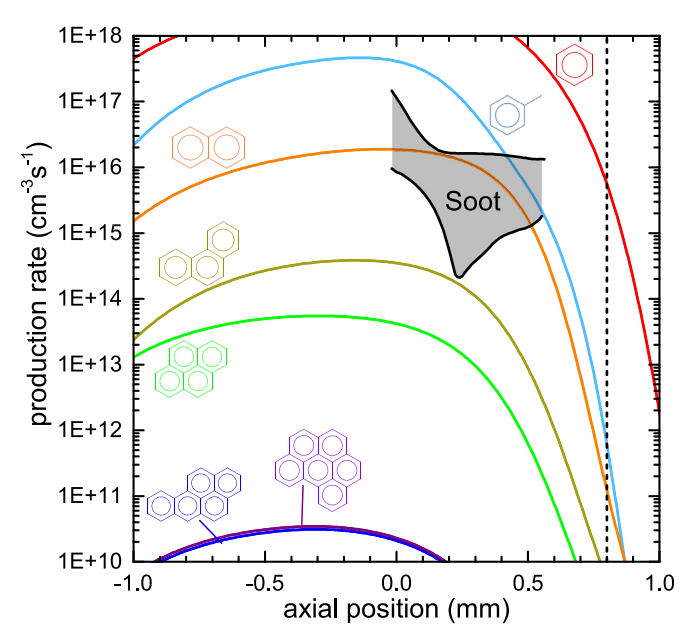


Fig. 3. Profiles of soot nucleation rate calculated under the hypothesis of monodisperse size: the shaded area is bracketed by assuming a coagulation efficiency of either 2% for the lower solid line or 100% for the upper solid line. Profiles of dimerization rate (colored lines) of several PAHs via kinetic theory of self-collisions and a representative benzene-toluene clustering (turquoise line) calculated by assuming 1% collision efficiency. (For interpretation of the references to color in this figure legend, the reader is referred to the web version of this article.)

parts as predicted by all the tested chemistry models (e.g., [55]). Even if the sampling collection method promoted the conversion of short-lived radicals to their stable species counterparts, the resulting error in the quantification of what are assumed to be stable species in the flame would be negligible. Conversely, even the detected stable molecules, such as ring-stabilized aromatic compounds, can become highly reactive and turned into an aryl radical through radical-promoted chemistry, such as H-abstraction, within the flame. Thus, the identification of these stable species does not preclude the applicability of radical-based models of soot nucleation [20,24].

Soot number concentration across the flame is in the range of 10^{12} – 10^{13} cm⁻³ (Fig. 2), where the illustrated range is bounded by values calculated assuming either particle monodispersity (lower solid black line) or a lognormal size distribution with relative standard deviation σ = 0.25 (upper dashed black line). Notably, the soot number concentration both at the "high-temperature" inception, close to the flame, and in the secondary, "low-temperature" nucleation stage (near the GSP), exceeds that of the larger PAHs by at least one order of magnitude. This finding suggests that only small aromatic compounds are able to control kinetically the nucleation of soot, if PAH dimerization is the first nucleation step, as broadly reported [17,20–24].

Considering the disparity in the molar abundances of soot as compared to larger PAHs like pyrene or coronene, which are often postulated as putative precursors to soot [17], we sought to evaluate soot production rate against possible (poly)aromatic dimerization rates. In the ensuing discussion, we will consider the formation of the dimer or cluster of two aromatic compounds to mark the formation of soot, even though much additional growth is required for the cluster to develop the properties of the solid phase. Using Eqs. (4)–(7), we compare the inception rate of soot with that of dimerization or clustering of aromatic compounds in Fig. 3. As explained in the section on data analysis, we calculate: i) soot nucleation rates via a governing equation for the soot number concentration, informed by measurements along the

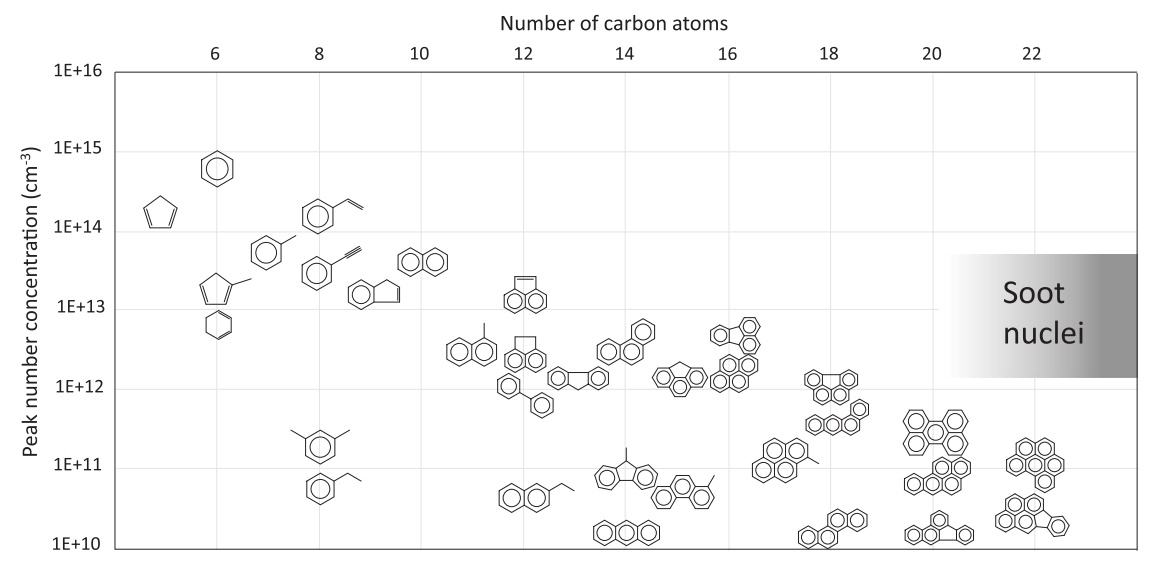


Fig. 4. A compendium of the results of peak number concentration of PAHs and soot in a variety of flame conditions at temperatures between 1200 K and 2000 K.

axis-symmetric flow field, that accounts for nucleation and particle transport (e.g., particle drift down a temperature gradient and diffusion due to Brownian motion) in the limiting cases of unity and 2% coagulation efficiencies; and ii) PAH dimerization (i.e., selfcollision) rate calculated according to the gas kinetic theory based on an interpolation of the measured PAH concentrations. Only aromatics containing one or two rings exhibit formation rates comparable to that of soot, whereas the formation rates and number concentration of large 4-6-ring-PAHs are too low to account for it. Moreover, the dimerization/clustering of larger PAHs would have had to be irreversible for the rates to be adequately high [26,66,67]. In other words, the rate-limiting step in the sequence that ultimately controls the nucleation rate appears to be the formation of either single-ring aromatic compounds, possibly with a methyl side chain, or, at most, two-ring aromatic compounds through this physicochemical clustering route. Other clustering options such as benzene-naphthalene and toluene-naphthalene are potentially viable. It is likely that in view of the high volatility of these compounds, the nature of the clustering is chemical rather than physical for the dimer to be stable at the high temperatures of flames [20,24,26].

Then, how can one reconcile the presence of PAHs of several hundred Da in the ordered stacks and disordered clusters that constitute soot nanoparticles, as indirectly and directly revealed by several studies on soot particle structure that find platelets of large polyaromatic compounds [13,22,23,68-71]? We do not discount the fact that larger PAHs play a role in the nucleation of soot, but the findings in Fig. 3 indicate that the very early stage of soot nucleation stems from aromatic structures that are smaller than those observed in mature soot. A plausible explanation is that large PAHs are short-lived intermediates that do not affect the very onset of nucleation, at least when the parent fuel is neither aromatic nor cyclic, as the case is for our study. The concentration of large PAHs is small as a consequence of a steady-state condition for this family of intermediates, which prevails if production rate and destruction rate are both large and comparable, so that the net production rate is very small (e.g., [16]). The ultimate fate of these larger aromatic compounds is to adsorb quickly on the initial dimers, leading to much larger peri-condensed PAHs with the necessary resonance stabilization that prevents their fragmentation. In this way, they certainly participate in the overall growth of the soot particle [24]. On the basis of the present data, we cannot address the detailed mechanisms that allow the dimers of small aromatics to stabilize, possibly via bridge-forming reactions [26,72], to overcome kinetic and thermodynamic constraints, and the subsequent clustering leading to the large PAHs that have been observed in microscopic analysis of soot nanoparticles. Considering the long-standing hypothesis that chemical bond-building and clustering of relatively *large* aromatic systems such as pyrene triggered incipient soot [17,19–23], the present finding that only *small* aromatic structures could support early soot formation rates from non-aromatic fuels is noteworthy.

This finding could be narrowed down perhaps to only single ring aromatic compounds based on the following considerations. In the first place, the assumption of 1% sticking probability for the aromatic dimerization rate is very generous for species smaller than pyrene [22,59,73]. Even the near-irreversible collision between a PAH molecule and a PAH radical [26] must consider small aromatic compounds because of the low concentration of radicals predicted by the kinetic models. On the other hand, the assumption of monodispersity of soot particles is reasonable only in the high-temperature nucleation zone but may become progressively weaker, as the particles evolve on their path towards the stagnation plane, as a result of concurring coagulation and the occurrence of secondary low-temperature nucleation. For a fixed measured volume fraction and light scattering coefficient, polydispersity would increase the coagulation term, since the number concentration of a polydisperse population is larger than that of a monodisperse one (Fig. 2), thereby increasing the calculated soot nucleation rate. This effect would be only partially compensated by the concurrent decrease in the average collision cross-section (i.e., K_{coll}) with increasing polydispersity at given volume fraction and light scattering coefficient. Additionally, subnanometer-size particles would be at number concentrations considerably larger than the ones inferred by optical measurements since their number is brought down by growth, following multiple coagulation steps. Thus, the number production rate of the smallest clusters/soot nuclei is expected to be much larger; i.e., the conclusion that only small ringed structures could support this growth stands and may be restricted to single-ringed aromatic compounds. Taken together, these considerations would yield a further increase in the soot nucleation profile and a decrease in the molecular dimerization rates, possibly precluding even the role of two-ring aromatic compounds in seeding the nucleation stage and indicating singleringed aromatic compounds as the dominant source of soot nucleation.

A compendium of the results of peak number concentrations of PAHs and soot is shown in Fig. 4. The schematic diagram considers additional results in different diffusion and partially premixed flames whose maximum temperatures span an interval of approximately 300 K [31-33] and in a substantially different combustion environments, such as a premixed flame where soot is formed at an approximately constant temperature of ~1680 K in the postflame region [38,74–76]. As expected, there is a systematic trend of decreasing concentration with increasing PAH size (i.e., number of carbon atoms) that is experimentally quantified while retaining at the same time a spatially resolved characterization of the flame structure. Some outliers in the grid (e.g., anthracene or chrysene), detected at concentration levels approaching the detection limit of the technique (~1 ppb / 10¹⁰ particles/cm³), suggest that some elongated PAHs are either generated less efficiently or are more readily converted to larger species and eventually to soot particles by comparison with peri-condensed PAHs. The lack of detection of even heavier aromatics implies that they are present at concentration levels that are lower than the detection limit of the diagnostics.

The important implication of the present findings is that good predictions of the consumption of the parent fuel components and the formation of single- and double-ringed aromatic structures and acetylene may be sufficient to enable modeling of soot inception rates, at least in flames fueled by non-cyclic aliphatic fuel components. Efforts to capture the intermediate growth to larger aromatic structures are not necessary from this perspective, even though large aromatic compounds remain important with respect to the overall soot growth as they adsorb on the soot nuclei and get incorporated in the final soot structure [71]. The implications of these findings on soot modeling apply to diverse combustion environments, from premixed sources to diffusion-controlled environments.

5. Conclusion

The novel technique developed here enabled quantitative analyses of large aromatic structures (up to 6-rings) at mole fractions as low as ppb in flames for the first time. The technique allows us to search for all isomeric species for a given molecular weight and, consequently, encompasses both 6-membered ring and 5-membered ring, as well as poly-alkylated aromatic species. Such a capability, coupled with the simultaneous measurement of soot particle size, number concentration, and volume fraction by optical techniques, provided the sequential evolution from the parent fuel molecule to soot. The approach preserved the spatial resolution necessary to resolve the flame structure and can be applied to a variety of flame environments, including high-pressure flames and the canonical premixed flames that have traditionally been the battleground of soot formation studies. Only the smallest aromatics are present in flame at sufficiently large number concentrations to account for soot nucleation, which suggests that large aromatic systems are not the key intermediates to incipient soot clusters. An overview of the flame structure confirms the expected trend of a systematic decrease in concentration with increasing PAH size. The methods and insights presented here should improve the description of soot formation rates from a multitude of sources.

Declaration of Competing Interest

The authors declare that they have no known competing financial interests or personal relationships that could have appeared to influence the work reported in this paper.

Acknowledgments

K.G. and A.G. acknowledge the support of the National Science Foundation (CBET-1853150) and Yale University. A.J.S. acknowledges the support of Yale University and the NSF Graduate Research Fellowship. Authors declare no competing interests.

Supplementary materials

Supplementary material associated with this article can be found, in the online version, at doi:10.1016/j.combustflame.2020.08.029.

References

- [1] J.S. Lighty, J.M. Veranth, A.F. Sarofim, Combustion aerosols: factors governing their size and composition and implications to human health, J. Air Waste Manag. Assoc. 50 (2000) 1565–1618.
- [2] N.A.H. Janssen, M.E. Gerlofs-Nijland, T. Lanki, R.O. Salonen, F.R. Cassee, G. Hoek, P. Fischer, B. van Bree Brunekreef, M. Krzyzanowski, WHO Report, World Health Organization, Copenhagen, Denmark 2012.
- [3] B. Frank, R. Schlogl, D.S. Su, Diesel soot toxification, Environ. Sci. Technol. 47 (2013) 3026–3027.
- [4] D. Shindell, G. Faluvegi, Climate response to regional radiative forcing during the twentieth century, Nat. Geosci. 2 (2009) 294–300.
- [5] T.C. Bond, S.J. Doherty, D.W. Fahey, P.M. Forster, T. Berntsen, B.J. DeAngelo, M.G. Flanner, S. Ghan, B. Kärcher, D. Koch, S. Kinne, Y. Kondo, P.K. Quinn, M.C. Sarofim, M.G. Schultz, M. Schulz, C. Venkataraman, H. Zhang, S. Zhang, N. Bellouin, S.K. Guttikunda, P.K. Hopke, M.Z. Jacobson, J.W. Kaiser, Z. Klimont, U. Lohmann, J.P. Schwarz, D. Shindell, T. Storelvmo, S.G. Warren, C.S. Zender, Bounding the role of black carbon in the climate system: A scientific assessment, J. Geophys. Res. Atmos. 118 (2013) 5380–5552.
- [6] R.K. Chakrabarty, N.D. Beres, H. Moosmüller, S. China, C. Mazzoleni, M.K. Dubey, L. Liu, M.I. Mishchenko, Soot superaggregates from flaming wildfires and their direct radiative forcing, Sci. Rep. 4 (2014) 5508.
- [7] International Energy Outlook 2018 (2018), https://www.eia.gov/outlooks/ieo/.
- [8] A. Nel, T. Xia, L. Madler, N. Li, Toxic potential of materials at the nanolevel, Science 311 (2006) 622–627.
- [9] G. Oberdörster, E. Oberdörster, J. Oberdörster, Nanotoxicology: an emerging discipline evolving from studies of ultrafine particles, Environ. Health Perspect. 113 (2005) 823–839.
- [10] P. Pedata, T. Stoeger, R. Zimmermann, A. Peters, G. Oberdorster, A. D'Anna, Are we forgetting the smallest, sub 10nm combustion generated particles? Part Fibre Toxicol. 12 (2015) 10–13.
- [11] P. Ehrenfreund, S.B. Charnley, Organic molecules in the interstellar medium, comets, and meteorites: a voyage from dark clouds to the early earth, Annu. Rev. Astron. Astrophys. 38 (2000) 427–483.
- [12] T. Henning, F. Salama, Carbon in the universe, Science 282 (1998) 2204-2210.
- [13] B.S. Haynes, H.G. Wagner, Soot Formation, Prog. Energy Combust. Sci. 7 (1981) 229–273.
- [14] M. Frenklach, D.W. Clary, W.C. Gardiner, S.E. Stein, Detailed kinetic modeling of soot formation in shock-tube pyrolysis of acetylene, Symp. (Int.) Combust. 20 (1985) 887–901.
- [15] K.H. Homann, Formation of large molecules, particulates and ions in premixed hydrocarbon flames; Progress and unresolved questions, Symp. (Int.) Combust. 20 (1985) 857–870.
- [16] I. Glassman, R.A. Yetter, Combustion, Academic Press, New York, NY, 1977.
- [17] M. Frenklach, H. Wang, Detailed modeling of soot particle nucleation and growth, Symp. (Int.) Combust. 23 (1991) 1559–1566.
- [18] J.A. Miller, C.F. Melius, Kinetic and thermodynamic issues in the formation of aromatic compounds in flames of aliphatic fuels, Combust. Flame 91 (1992) 21–39
- [19] H. Richter, J.B. Howard, Formation of polycyclic aromatic hydrocarbons and their growth to soot a review of chemical reaction pathways, Prog. Energy Combust. Sci. 26 (2000) 565–608.
- [20] A. D'Anna, A. Violi, A kinetic model for the formation of aromatic hydrocarbons in premixed laminar flames, Symp. (Int.) Combust. 27 (1998) 425–433.
- [21] M. Frenklach, Reaction mechanism of soot formation in flames, Phys. Chem. Chem. Phys. 4 (2002) 2028–2037.
- [22] A. D'Anna, Combustion-formed nanoparticles, Proc. Combust. Inst. 32 (2009) 593–613.
- [23] H. Wang, Formation of nascent soot and other condensed-phase materials in flames, Proc. Combust. Inst. 33 (2011) 41–67.
- [24] K.O. Johansson, M.P. Head-Gordon, P.E. Schrader, K.R. Wilson, H.A. Michelsen, Resonance-stabilized hydrocarbon-radical chain reactions may explain soot inception and growth, Science 361 (2018) 997–1000.
- [25] Y. Wang, S.H. Chung, Soot formation in laminar counterflow flames, Prog. Energy Combust. Sci. 74 (2019) 152–238.
- [26] M. Frenklach, A.M. Mebel, On the mechanism of soot nucleation, Phys. Chem. Chem. Phys. 22 (2020) 5314–5331.

- [27] L. Zhao, R.I. Kaiser, W. Lu, B. Xu, M. Ahmed, A.N. Morozov, A.M. Mebel, A.H. Howlader, S.F. Wnuk, Molecular mass growth through ring expansion in polycyclic aromatic hydrocarbons via radical-radical reactions, Nat. Commun. 10 (2019) 1–7.
- [28] S.E. Stein, A. Fahr, High-temperature stabilities of hydrocarbons, J. Phys. Chem. 89 (1985) 3714–3725.
- [29] N. Hansen, T.A. Cool, P.R. Westmoreland, K. Kohse-Hoinghaus, Recent contributions of flame-sampling molecular-beam mass spectrometry to a fundamental understanding of combustion chemistry, Prog. Energy Combust. Sci. 35 (2009) 168-191.
- [30] F. Qi, Combustion chemistry probed by synchrotron VUV photoionization mass spectrometry, Proc. Combust. Inst 34 (2013) 33–63.
- [31] F. Carbone, K. Gleason, A. Gomez, Pressure effects on incipiently sooting partially premixed counterflow flames of ethylene, Proc. Combust. Inst. 36 (2017) 1395–1402
- [32] K. Gleason, F. Carbone, A. Gomez, Effect of temperature on soot inception in highly controlled counterflow ethylene diffusion flames, Combust. Flame 192 (2018) 283–294.
- [33] F. Carbone, F. Cattaneo, A. Gomez, Structure of incipiently sooting partially premixed ethylene counterflow flames, Combust. Flame 162 (2015) 4138–4148.
- [34] U. Struckmeier, P. Oßwald, T. Kasper, L. Böhling, M. Heusing, M. Köhler, A. Brockhinke, K. Kohse-Höinghaus, Sampling probe influences on temperature and species concentrations in molecular beam mass spectroscopic investigations of flat premixed low-pressure flames, Z. Phys. Chem. 223 (2009) 503-537
- [35] V. Gururajan, F.N. Egolfopoulos, K. Kohse-Höinghaus, Direct numerical simulations of probe effects in low-pressure flame sampling, Proc. Combust. Inst. 35 (2015) 821–829.
- [36] J.C. Biordi, Molecular beam mass spectrometry for studying the fundamental chemistry of flames, Prog. Energy Combust. Sci. 3 (1977) 151–173.
- [37] N. Hansen, R.S. Tranter, K. Moshammer, J.B. Randazzo, J.P.A. Lockhart, P.G. Fugazzi, T. Tao, A.L. Kastengren, 2D-imaging of sampling-probe perturbations in laminar premixed flames using Kr X-ray fluorescence, Combust. Flame 181 (2017) 214–224.
- [38] F. Carbone, K. Gleason, A. Gomez, Probing gas-to-particle transition in a moderately sooting atmospheric pressure ethylene/air laminar premixed flame. Part I: gas phase and soot ensemble characterization, Combust. Flame 181 (2017) 315–328.
- [39] L. Figura, A. Gomez, Structure of incipiently sooting ethylene-nitrogen counterflow diffusion flames at high pressures, Combust. Flame 161 (2014) 1587–1603.
- [40] L. Figura, F. Carbone, A. Gomez, Challenges and artifacts of probing highpressure counterflow laminar diffusion flames, Proc. Combust. Inst. 35 (2015) 1871–1878.
- [41] D.L. Plata, A.J. Hart, C.M. Reddy, P.M. Gschwend, Early evaluation of potential environmental impacts of carbon nanotube synthesis by chemical vapor deposition, Environ. Sci. Technol. 43 (2009) 8367–8373.
- [42] D.L. Plata, E.R. Meshot, C.M. Reddy, A.J. Hart, P.M. Gschwend, Multiple alkynes react with ethylene to enhance carbon nanotube synthesis, suggesting a polymerization-like formation mechanism, ACS Nano 4 (2010) 7185–7192.
- [43] M.V. Heitor, A.L.N. Moreira, Thermocouples and sample probes for combustion studies, Prog. Energy Combust. Sci. 19 (1993) 259–278.
- [44] G.D. Nessim, M. Seita, D.L. Plata, K.P. OBrien, A. John Hart, E.R. Meshot, C.M. Reddy, P.M. Gschwend, C.V. Thompson, Precursor gas chemistry determines the crystallinity of carbon nanotubes synthesized at low temperature, Carbon N Y 49 (2011) 804–810.
- [45] C. Aeppli, C.A. Carmichael, R.K. Nelson, K.L. Lemkau, W.M. Graham, M.C. Redmond, D.L. Valentine, C.M. Reddy, Oil weathering after the Deepwater Horizon disaster led to the formation of oxygenated residues, Environ. Sci. Technol. 46 (2012) 8799–8807.
- [46] R.K. Nelson, B.M. Kile, D.L. Plata, S.P. Sylva, L. Xu, C.M. Reddy, R.B. Gaines, G.S. Frysinger, S.E. Reichenbach, Tracking the weathering of an oil spill with comprehensive two-dimensional gas chromatography, Environ. Forens. 7 (2006) 33–44.
- [47] P.B. Kuhn, B. Ma, B.C. Connelly, M.D. Smooke, M.B. Long, Soot and thin-filament pyrometry using a color digital camera, Proc. Combust. Inst. 33 (2011) 743–750.
- [48] S. Torok, V.B. Malmborg, J. Simonsson, A. Eriksson, J. Martinsson, M. Mannazhi, J. Pagels, P.E. Bengtsson, Investigation of the absorption Angstrom exponent and its relation to physicochemical properties for mini-CAST soot, Aerosol. Sci. Technol. 52 (2018) 757–767.
- [49] R.C. Millikan, Optical properties of soot, J. Opt. Soc. Am. 51 (1961) 698–699.
- [50] B. Ma, M.B. Long, Absolute light calibration using S-type thermocouples, Proc. Combust. Inst. 34 (2013) 3531–3539.

- [51] A. D'Alessio, Laser light scattering and fluorescence diagnostics of rich flames produced by gaseous and liquid fuels, in: D.C. Siegla (Ed.), Particulate Carbon, Springer, 1981, pp. 207–259.
- [52] M.P. Bogaard, A.D. Buckingham, R.K. Pierens, A.H. White, Rayleigh scattering depolarization ratio and molecular polarizability anisotropy for gases, J. Chem. Soc. Farad. Trans. 1: Phys. Chem. Condens. Phases 74 (1978) 3008–3015.
- [53] G. Sutton, A. Levick, G. Edwards, D. Greenhalgh, A combustion temperature and species standard for the calibration of laser diagnostic techniques, Combust. Flame 147 (2006) 39–48.
- [54] H.A. Michelsen, P.E. Schrader, F. Goulay, Wavelength and temperature dependences of the absorption and scattering cross sections of soot, Carbon N Y 48 (2010) 2175–2191.
- [55] Y. Wang, A. Raj, S.H. Chung, A PAH growth mechanism and synergistic effect on PAH formation in counterflow diffusion flames, Combust. Flame 160 (2013) 1667–1676
- [56] R.J. Kee, F.M. Rupley, E. Meeks, J.A. Miller, Chemkin-III: a Fortran chemical kinetics package for the analysis of gas-phase chemical and plasma kinetics, Sand. Nat.l. Lab. (1996) Report No. SAND 96-8216.
- [57] A.E. Lutz, R.J. Kee, J.F. Grcar, F.M. Rupley, OPPDIF: a Fortran program for computing opposed flow diffusion flames, Sand. Natl. Lab. (1997) Report No. SAND 96-8243.
- [58] W.L. Grosshandler, RADCAL: a Narrow-band model for radiation calculations in a combustion environment, NIST Technical Note 1402. NIST 1993.
- [59] A. D'Alessio, A.C. Barone, R. Cau, A. D'Anna, P. Minutolo, Surface deposition and coagulation efficiency of combustion generated nanoparticles in the size range from 1 to 10nm, Proc. Combust. Inst. 30 (2005) 2595–2603.
- [60] D. Hou, D. Zong, C.S. Lindberg, M. Kraft, X. You, On the coagulation efficiency of carbonaceous nanoparticles, J. Aerosol. Sci. 140 (2020) 105478.
- [61] S.K. Friedlander, Smoke, Dust and Haze: Fundamentals of Aerosol Behavior, John Wiley & Sons Inc, 1977.
- [62] Z. Li, H. Wang, Drag force, diffusion coefficient, and electric mobility of small particles. II. Application, Phys. Rev. E (2003) 68.
- [63] Z. Li, H. Wang, Thermophoretic force and velocity of nanoparticles in the free molecule regime, Phys. Rev. E 70 (2004) 11.
- [64] P.D. Neufeld, A.R. Janzen, R.A. Aziz, Empirical equations to calculate 16 of the transport collision integrals $\Omega(I,s)^*$ for the Lennard–Jones (12–6) potential, J. Chem. Phys. 57 (1972) 1100–1102.
- [65] H. Bockhorn, F. Fetting, A. Heddrich, U. Meyer, G. Wannemacher, Particle sizing of soot in flat pre-mixed hydrocarbon oxygen flames by light scattering, J. Aerosol Sci. 19 (1988) 591–602.
- [66] H. Miller, K.C. Smyth, W.G. Mallard, J. Houston Miller, K.C. Smyth, W.G. Mallard, Calculations of the dimerization of Aromatic Hydrocarbons: implications for soot formation, Symp. (Int.) Combust. 20 (1984) 1139–1147.
- [67] N.A. Eaves, S.B. Dworkin, M.J. Thomson, The importance of reversibility in modeling soot nucleation and condensation processes, Proc. Combust. Inst. 35 (2015) 1787–1794.
- [68] E.M. Adkins, J.H. Miller, Extinction measurements for optical band gap determination of soot in a series of nitrogen-diluted ethylene/air non-premixed flames, Phys. Chem. Chem. Phys. 17 (2015) 2686–2695.
- [69] K. Yehliu, R.L. Vander Wal, A.L. Boehman, Development of an HRTEM image analysis method to quantify carbon nanostructure, Combust. Flame 158 (2011) 1837–1851.
- [70] M.L. Botero, Y. Sheng, J. Akroyd, J. Martin, J.A.H. Dreyer, W. Yang, M. Kraft, Internal structure of soot particles in a diffusion flame, Carbon N Y 141 (2019) 635–642.
- [71] H. Miller, A. Vertes, R.J. Golden, A.R. Korte, The molecular composition of soot, Angew. Chem. Int. Ed. (2020) 2–9.
- [72] M.R. Kholghy, N.A. Eaves, A. Veshkini, M.J. Thomson, The role of reactive PAH dimerization in reducing soot nucleation reversibility, Proc. Combust. Inst. 37 (2019) 1003–1011.
- [73] A. Raj, M. Sander, V. Janardhanan, M. Kraft, A study on the coagulation of polycyclic aromatic hydrocarbon clusters to determine their collision efficiency, Combust. Flame 157 (2010) 523–534.
- [74] F. Carbone, S. Moslih, A. Gomez, Probing gas-to-particle transition in a moderately sooting atmospheric pressure ethylene/air laminar premixed flame. Part II: molecular clusters and nascent soot particle size distributions, Combust. Flame 181 (2017) 329–341.
- [75] F. Carbone, M.R. Canagaratna, A.T. Lambe, J.T. Jayne, D.R. Worsnop, A. Gomez, Exploratory analysis of a sooting premixed flame via on-line high resolution (APi-TOF) mass spectrometry, Proc. Combust. Inst. 37 (2019) 919–926.
- [76] K. Gleason, F. Carbone, A.J. Sumner, B.D. Drollette, D.L. Plata, A. Gomez, A novel method for spatiallyresolved quantitation of large polycyclic aromatic hydrocarbons in laminar sooting flames, 11th U. S. National Combustion Meeting, Pasadena, California (2019) March 24–27.